communications medicine

A Nature Portfolio journal

Article

https://doi.org/10.1038/s43856-026-01431-x

A longitudinal comparative analysis of serum metabolomic signatures in children with SARS-CoV-2 infection and MIS-C

A. Lo Vecchio[1,7] ✉, V. Discepolo[1,2,7], L. Pierri[1], A. Catzola[1], M. Lombardi[3,4,5], A. Colucci[6], M. Poeta[1], E. Bruzzese[1], J. Troisi[3,4,6] & A. Guarino[1] ✉

Abstract

Background SARS-CoV-2 infection usually has a mild course in childhood, yet few children develop a Multisystem Inflammatory Syndrome (MIS-C). Several metabolic pathways have been found to be dysregulated in adults with COVID-19, yet data are lacking in children. Here we investigate serum metabolomic features of children with COVID-19 in relation to age, sex and both clinical and biochemical severity.

Methods We carried out a prospective observational comparative cohort study enrolling 92 children (48 M, mean age 3.69 ± 5.1 years) with acute SARS-CoV-2 infection and 7 with MIS-C along with 41 age- and sex-matched controls. Sera collected at admission, acute phase, discharge and remission were analyzed by Gas Chromatography Mass Spectroscopy.

Results Here we identify a distinct signature featuring inflammation, reactive oxygen species and glicerolipids pathways in children with acute SARS-CoV-2 infection compared to controls (permutation test p = 0.0015). Metabolomic profile changes are associated with age, disease status and disease severity, while a normalization of these changes is observed at disease resolution. MIS-C children showed a unique signature compared to age-/sex-matched COVID-19 patients or controls.

Conclusions Pediatric COVID-19 has a characteristic metabolomic signature featuring glucose and aminoacid metabolism, that varies with age and disease phenotype. Our study supports the value of metabolomics to unveil pathways related to host-viral interaction that may also help identify early predictors of disease evolution.

Plain language summary

After the COVID-19 pandemic, despite the wide-spread vaccination campaigns, we have been witnessing multiple surges of SARS-CoV-2 epidemics around the globe that, albeit less severe, are still contributing significantly to morbidity in the general population. Children are frequently affected, and in rare cases may develop a complication known as Multisystem Inflammatory Syndrome that may have a critical course. In this study we have investigated changes in blood metabolites resulting from the interaction between the SARS-CoV-2 and children, revealing that their variations are associated with age and disease severity. Our study could help identifying early markers that may predict disease evolution.

The clinical presentation of severe acute respiratory syndrome coronavirus 2 (SARS-CoV-2) infection is highly variable, ranging from a condition of asymptomatic infection to a severe and life-threatening coronavirus disease (COVID-19).

Acute SARS-CoV-2 infection in children usually has a mild clinical presentation, similar to other acute viral respiratory infections, with a low complication and mortality rate compared to adults[1,2]. However, some risk factors like older age, comorbidities, and co-infections have been linked to a worse outcome[3].

Furthermore, approximately 2–4 weeks after exposure to SARS-CoV-2, a small proportion of children develop a hyperinflammatory response known as multisystem inflammatory syndrome in children (MIS-C), that causes multiple organ disfunction, requires intensive care in 60–80% of affected children and leads to death about 2–5% of them ref. 4. In addition, a growing proportion of children and adolescents is complaining long-term symptoms and complications temporarily related to SARS-CoV-2[5].

Factors that predispose a subject to severe outcomes during acute infection, as well as to the development of long-term complications, are still

[1]Section of Pediatrics, Department of Translational Medical Sciences, Clinical Research Center DEMeTra, University of Naples Federico II, Naples, Italy. [2]European Laboratory for the Investigation of Food Induced Diseases (ELFID) and Centro di Ingegneria Genetica (CeInGe), University of Naples Federico II, Naples, Italy. [3]Theoreo srl, Montecorvino Pugliano (SA), Italy. [4]EIM-European Institute of Metabolomics Foundation, Baronissi (SA), Italy. [5]Department of Chemistry and Biology "A. Zambelli", University of Salerno, Fisciano (SA), Italy. [6]Department of Medicine Surgery and Dentistry "Scuola Medica Salernitana", University of Salerno, Baronissi (SA), Italy. [7]These authors contributed equally: A. Lo Vecchio, V. Discepolo. ✉e-mail: andrea.lovecchio@unina.it; alfguari@unina.it

under investigation, and might be ascribed to genetic predisposition, presence of co-morbidities and host immune response to infection. The detrimental impact that obesity, diabetes, and aging have on clinical outcomes suggests a strong correlation between metabolic disturbances and severe COVID-19 that deserves to be further explored.

Untargeted metabolomic approach, that investigates the continuous exchanges of small molecules between tissues and fluids, is commonly used to examine biological pathways associated with disease, generate mechanistic hypotheses, and identify specific metabolic signatures for diagnosis and prognostication. This approach has been used as a component of the omics toolkit in biomedical COVID-19 research, to identify dysregulation of metabolic pathways during the disease's progression[6]. Importantly, it can contribute to understand biological pathways associated with host-viral interaction.

Several metabolic pathways seem to be dysregulated by the host-viral interaction in adults with COVID-19. The main metabolic perturbations in SARS-CoV-2 infection included cellular amino acids metabolism, used as fuel for viral proliferation[7,8] and arachidonic acid, recognized as endogenous antiviral lipid[9] On the other hand, a host-related response to infection may result in a perturbation of tryptophan-nicotinamide pathway implicated in inflammatory signaling together with cytosine, as a coordinator of metabolism of SARS-CoV-2-infected cells[10] porphyrin metabolism implicated in multi-organs damaging[11], and other molecules implicated in platelet degranulation and complement system pathways as well as in macrophage deregulation/ROS balances[6]

A recent meta-analysis by Pang and colleagues identified the dysregulation of six separate metabolomic pathways in adult patients with COVID-19, including tricarboxylic acid cycle, short-chain fatty acid and aminoacidic metabolism, and revealed a correlation between metabolic alteration and disease severity[12].

The slackening of restrictive measures, reopening of schools and social activities, and the slower rate of vaccination in the pediatric population compared to adults, left the pediatric population as the main target for SARS-CoV-2 infection worldwide. In a scenario featuring such an increasing number of infected children, identifying those who may develop severe clinical outcomes or MIS-C might be of crucial importance for clinical management.

Table 1 | General characteristics of enrolled children

	Acute COVID ($n = 91$)	MIS-C ($n = 7$)	Healthy controls ($n = 41$)	p-value[#]
Sex, female (%)	43 (47.2)	4 (57.1)	16 (39.0)	0.553
Median age, years (IQR)	0.70 (0.15–4.8)	11.3 (6.5–11.9)	5.0 (0.54–13)	0.142
Ethnicity, caucasian (%)	89 (97)	7 (100)	39 (95)	0.621
Comorbidities, *n* (%)	23 (25.2)	2 (28.6)	–	0.847
Severe obesity	4 (4.4)	2 (28.6)	–	0.010
Genetic/metabolic disease	3 (3.3)	0 (0)	–	1.000
Haemato-oncological disease	2 (2.2)	0 (0)	–	1.000
Cardiological disease	3 (3.3)	0 (0)	–	1.000
Respiratory disease	5 (5.5)	0 (0)	–	1.000
Neurologic disease	4 (4.4)	0 (0)	–	1.000
Renal disease	2 (2.2)	0 (0)	–	1.000

COVID coronavirus disease, *MIS-C* multisystem inflammatory syndrome in children, *SARS-CoV-2* severe acute respiratory syndrome coronavirus 2.
[#]Fisher's exact test.

Little is known about metabolomics in children with COVID19[13]. Thus, a specific signature of SARS-CoV-2-infected children has not been identified yet, nor metabolomic profiles have been correlated with stage, phenotype, and severity of the disease. To this end, we designed a longitudinal cohort study to investigate the metabolomic fingerprint of Caucasian children with acute COVID-19 and MIS-C, and assess its variations according to the child's age, disease course and severity.

Our study reveals profound metabolomic changes in SARS-CoV-2-infected children associated with age, disease status and severity, that resolve upon disease resolution, unveiling pathways related to host-viral interaction. While MIS-C features a unique signature compared to age and sex-matched COVID-19 patients or controls. This approach may help identify predictors of disease evolution.

Materials and methods

Study population and definitions

Children aged between 1 month and 18 years, admitted at the Pediatric Infectious Diseases Unit of the University of Naples Federico II for symptomatic and laboratory confirmed SARS-CoV-2 infection or MIS-C, between April 2nd, 2020 and June 30th, 2021, were enrolled in the study. The hospital unit serves as referral center for the management of pediatric COVID-19 in the Campania Region, the most populous region in Southern Italy, and accepts children from emergency departments of other hospitals, as well as children directly referred by family pediatricians.

Diagnosis of SARS-CoV-2 infection was established in the presence of suggestive symptoms and a positivity of validated real-time reverse-transcriptase polymerase-chain-reaction (RT-PCR) assay in at least one respiratory specimen. MIS-C was diagnosed according to the Center for Disease Control and Prevention diagnostic criteria[14].

A group of age- and sex-matched healthy children, whose RT-PCR nasopharyngeal swab was negative for SARS-CoV-2, served as controls.

Study design and protocol

We designed a prospective longitudinal controlled cohort study to investigate the metabolomic profile in children with laboratory-confirmed SARS-CoV-2 infection, and to describe possible variations in accordance with the severity and the stage of the disease. In order to assess the degree of metabolic changes compared to normal, the results of COVID-patients' metabolomic analysis were compared to healthy controls.

Furthermore, the metabolomic profile of a small population of children with MIS-C was also evaluated and compared either with age- and sex-matched children with acute SARS-CoV-2 infection, or with controls.

Children aged 1 month to 18 years who consecutively accessed the pediatric infectious diseases unit of our institution during the study period were considered for enrollment. Those whose caregivers provided informed consent were included in the study protocol.

To minimize potential confounding effects on the metabolomic analysis, children with specific underlying conditions and/or undergoing treatments known to significantly influence the metabolomic profile—such as haemato-oncological diseases under chemotherapy, diabetic ketoacidosis, or dependence on parenteral nutrition—were excluded from participation. Neonates (<1 month), adults, or patients whose caregivers refused to sing, or formally withdrew their consent to the collection of scheduled biological samples, were excluded from the study.

At hospital admission, all patients underwent thorough clinical examination, laboratory workup, radiological evaluation if needed, nasopharyngeal swab and quantitative serological evaluation to confirm SARS-CoV-2 infection.

Laboratory work-up included complete cell blood count, liver and kidney panel, coagulation profile with D-dimer, inflammatory markers (IL-6, C-reactive protein-CRP, procalcitonin, PCT), ferritin, markers of myocardial injury (CK-MB and troponin). In addition, to assess possible co-infections, a microbiological work-up was performed, including: blood, urine and stool cultures, multiplex-PCR on nasal swab to search for respiratory viruses, and serology or antigen for bacteria (*Mycoplasma*

Table 2 | Clinical and laboratory features of enrolled children

	Acute COVID ($n = 91$)	MIS-C ($n = 7$)	p-value[#]
Symptoms, *n* (%)			
Fever	65 (70.6)	7 (100)	0.184
Cough	27 (29.3)	0 (0)	0.184
Conjunctivitis	2 (2.2)	1 (14.3)	0.070
Respiratory distress syndrome	8 (8.8)	0 (0)	1.000
Vomit	9 (9.8)	6 (85.7)	<0.001
Diarrhea	19 (20.6)	4 (57.1)	0.029
Abdominal pain	5 (5.4)	3 (42.8)	<0.001
Dysgeusia	3 (3.3)	0 (0)	1.000
Febrile seizures	3 (3.3)	0 (0)	1.000
Clinical severity[a]			
Mild	72 (79.3)	0 (0)	<0.001
Moderate	13 (14.1)	0 (0)	0.589
Severe	6 (6.5)	7 (100)	<0.001
Diagnosis, *n* (%)			
Positive SARS-CoV-2 nasopharyngeal swab	91 (100)	3 (43)	<0.001
Positive SARS-CoV-2 IgG antibodies	13 (14.3)	7 (100)	<0.001
Diagnosis of co-infections	12 (13.1)	1 (14.3)	0.934
Chest X-ray	63 (69.2)	7 (100)	0.186
Chest computed tomography	5 (5.5)	2 (28.6)	0.022
Markers of inflammation, mean (SD)			
C-reactive protein, mg/dL	9.8 (21.7)	242.4 (126)	<0.001
Procalcitonin, ng/mL	0.7 (2.2)	13.6 (7.8)	<0.001
Interleukin-6, pg/mL	206 (622)	135.5 (176.8)	0.382
Therapy, *n* (%)			
Paracetamol	65 (70.6)	7 (100)	0.184
Antibiotics	26 (28.2)	7 (100)	<0.001
Low-molecular-weight heparin	2 (2.2)	6 (85.7)	<0.001
Corticosteroids	4 (3.3)	7 (100)	<0.001
IVIG	1 (1.1)	7 (100)	<0.001
IL-1 antagonists	0 (0)	2 (28.6)	0.004
Complications, *n* (%)	6 (5.5)	4 (57)	<0.001
Severe interstitial Pneumonia	4 (4.4)	0 (0)	1.000
Encephalitis	1 (1.1)	0 (0)	1.000
Sepsis/septic shock	1 (1.1)	0 (0)	1.000
Abdominal surgery	0 (0)	2 (28.6)	0.004
Myocarditis	0 (0)	2 (28.6)	0.004
Clinical outcomes, *n* (%)			
Mean length of stay (SD)	6 (5.7)	16.1 (7.5)	<0.001
Intensive care unit admission	1 (1.1)	2 (28.6)	<0.001
Deaths	0 (0)	0(0)	1.000

COVID coronavirus disease, *MIS-C* multisystem inflammatory syndrome in children, *SARS-CoV-2* severe acute respiratory syndrome coronavirus 2, *IVIG* intravenous immunoglobulins, *IL-1* interleukin-1.

[#]Fisher's exact test.

[a]Severity of SARS-CoV-2-related disease was defined as follows:
Mild: children with mild symptoms, slightly altered inflammatory markers or lab tests, only requiring supportive treatment during hospitalization.
Moderate: children with persistent or long-lasting symptoms (i.e., fever, cough, diarrhea) and elevated inflammation markers, requiring treatment during hospitalization.
Severe: clinically ill patients, in most cases, presenting with very elevated inflammatory markers, pro-coagulative state and/or severe interstitial pneumonia who required specific COVID-19 treatment, including systemic steroids, low-molecular weight heparin, or other anti-inflammatory drugs.

pneumoniae, *Chlamydia pneumoniae*, Pneumococcus, and *Legionella Pneumophila*).

Based on clinical presentation, presence of comorbidities and laboratory tests, two independent investigators (A.L.V. and L.P.) retrospectively classified each patient into one of the following categories (Tables 1 and 2):

- *Mild*: children with mild symptoms, slightly altered inflammatory markers or lab tests, only requiring supportive treatment during hospitalization;
- *Moderate*: children with persistent or long-lasting symptoms (i.e., fever, cough, diarrhea) and elevated inflammatory markers, requiring treatment during hospitalization;
- *Severe*: clinically ill patients presenting in most cases with elevated inflammatory markers, pro-coagulative state and/or severe interstitial pneumonia who required specific COVID-19 treatment, including systemic steroids, low-molecular weight heparin, or other anti-inflammatory drugs.

All children fulfilling the criteria for MIS-C diagnosis ($n = 7$, Tables 1 and 2) showed a severe clinical presentation. Those children were included as a distinct population for the study purpose.

From patients whose caregivers agreed to participate to the study protocol, at the time of blood drawn for clinical purposes, an additional serum sample was collected and stored at −80 °C. The timing of sampling was classified according to the stage and severity of the diseases as follows:

- T1 (admission): at hospital admission for all children with mild/moderate presentation;
- T2 (critical): at the time of the most severe clinical features during hospitalization or at admission, only for those already severely ill at first examination;
- T3 (discharge): at hospital discharge, usually patients were still SARS-CoV-2 positive, but in stable clinical conditions not requiring hospitalization;
- T4 (follow-up): during a follow-up visit scheduled after the first nasopharyngeal swab negative for SARS-CoV-2 (median 40 days, interquartile range (IQR) 31–75) and including clinical and lab investigation at the same institution.

This study was undertaken in accordance with good clinical practice guidelines and the Declaration of Helsinki. The study protocol was approved by the Ethical Committee of the University of Naples Federico II (protocol number 226/21). Written informed consent was obtained from parents/caregivers and patients, if appropriate.

Statistical analysis

The STROBE checklist for cohort studies was used as a guideline to report data (Supplemental Content). Characteristics of the study population are reported in Tables 1 and 2. Continuous clinical and biochemical parameters were reported as mean and standard deviation (SD), or median and IQR, according to their distribution and compared using t-test or Mann–Whitney test, as appropriate. Categorical measures expressed as frequencies and percentages were compared using Fisher's exact test or $\chi 2$.

Two-sided $p < 0.05$ were considered significant for clinical and biochemical variables. Statistical analysis of metabolomic data was performed using R software version 4.1.0 (Foundation for Statistical Computing, Vienna, Austria).

Untargeted metabolomic analysis

Metabolomic analysis was conducted following a validated protocol by Troisi et al.[15], with slight adjustments. Serum metabolites were extracted using the MetaboPrep GC Kit (Theoreo srl, Montecorvino Pugliano, Italy), by vortexing 50 µL of each serum sample at 1250 rpm with the extraction solution for 30 min. The resulting 192 extracts were derivatized prior to analysis. Two microliters of the derivatized mixture were injected into a Shimadzu GC-2010 Plus system coupled with a single quadrupole mass spectrometer. Metabolite separation was achieved using a 30-meter CP-Sil 8 CB fused silica capillary column (0.25 mm i.d., 1.00 µm film thickness;

Agilent, J&W Scientific), operated with helium as the carrier gas at a constant linear velocity of 39 cm/s. The oven temperature was initially held at 100 °C for 1 min, ramped at 6 °C per minute to a final temperature of 320 °C, and maintained for an additional 2.33 min, totaling 40 min per run. The injector was operated with a split ratio of 1:5. Mass spectra were acquired in full scan mode (range: m/z 35–600) using electron impact ionization at 70 eV, with a scan speed of 3333 amu/sec and a solvent delay of 5 min.

To ensure analytical consistency and robust data quality, GC-MS runs were organized in batches of 25 samples, each subjected to a comprehensive quality control (QC) strategy. Every batch included four control types: (i) a solvent blank (2 µL hexane) to monitor contamination, (ii) a derivatized mix of 15 metabolite standards representing major biochemical classes (sugars, amino acids, fatty acids, organic acids, steroids), (iii) a pooled QC sample consisting of 2 µL aliquots from all study samples, and (iv) a technical replicate of one randomly chosen study sample.

Each batch was considered valid only if the following conditions were met: (1) no detectable peaks in the blank chromatogram, (2) retention of standard mix signal intensity within ±10% of expected values (normalized to the internal standard), (3) coefficient of variation (CV) < 15% across the 100 most intense peaks in the technical replicate, and (4) tight clustering of pooled QC samples within 5% total variance in a PCA model generated from all pooled QCs (see Supplementary Fig. 1). This multi-tiered control approach ensured high reproducibility across runs and minimized potential batch effects. A list of all metabolites is included in Supplementary Table 1.

Classification model building. Partial least square discriminant analysis (PLS-DA)[16] was performed on the internal standard peak area[17] normalized chromatogram using R software version 4.1.0 (Foundation for Statistical Computing, Vienna, Austria) with the IDE R-studio version 1.4.1717. Mean centering and unit variance scaling was applied for all analyses. Classes separation was archived by PLS-DA, which is a supervised method using linear combinations of original variables (*X*) to extract the information that can predict class membership (Y). Classification and cross-validation were also performed by means of the wrapper function included in the caret package[18]. Moreover, a permutation test assessing the class-discriminating statistical significance was performed. For each of the 1000 tested permutations, a PLS-DA model was built between the metabolites data (*X*) and the permuted class labels (Y) using the best performing number of components determined by cross-validation. To assess the results generalizability a leave-3-out cross-validation was performed[19]. Each round of cross-validation involves partitioning of the sample of data into two complementary subsets. A discriminant model was trained on the higher dimension subset and validated on the other. To increase the cross-validation robustness, multiple rounds of training-testing steps were performed until all possible ways to divide the original dataset were explored. To manage the class imbalance, reducing its effects on the sensitivity and specificity of the class assignment, the metacost algorithm[20] was used. A cost matrix was built according to the number of elements in each class.

Variable importance in projection (VIP) scores were calculated for each component. For each relevant metabolite, the human metabolome database (HMDB) ID number was determined. Metabolites with higher VIP-score were further confirmed with an independent analytical standard as reported in the Metabolomics Standard Initiative (level MSI = 1)[21]. Metabolic pathway involvement was also evaluated using the MetPa tool[22].

The pathway analysis was performed combining the results from pathway enrichment analysis with pathway topology analysis according to Xia and Wishart[22]. The analysis was based on the KEGG metabolic pathways as the backend knowledge base included in the web application, based on the MetPa algorithm. By means of the over-representation analysis, we first tested if compounds involved in a particular pathway were enriched compared to random hits. This evaluation was based on the hypergeometric test. Moreover, to take into consideration the structural information of the pathways, a topology analysis was performed using the betweenness centrality as a measure of node centrality to estimate node importance. Because several pathways were tested at the same time, the statistical *p*-values from enrichment analysis were adjusted for multiple testing with the false discovery rate (FDR) method. The Impact is the pathway impact value calculated from pathway topology analysis.

Results

Characteristics of the study cohort

To gain insight into the metabolomic characteristics of COVID-19 patients with different disease phenotypes, a cohort of 99 pediatric patients (92 with acute SARS-CoV-2 infection and 7 with MIS-C) and 41 healthy controls were enrolled. The demographic, clinical and laboratory characteristics of the study population are reported in Tables 1 and 2.

All patients were enrolled during the first three pandemic waves. Although viral genotyping was not available for single patients, the ancestral B.1 and B1.1. SARS-CoV-2 genotypes and B.1.1.7 (Alpha) variant were prevalent in the region during the study period, and other variants, such as B.1.177x (Spanish), C.18 and P.1 (Gamma) sporadically circulated in less than 5% of the local population (Supplementary Table 2).

At the time of enrollment, none of the patients had received vaccination against SARS-CoV-2. The total cohort samples ($n = 197$) used for each individual assay are outlined in Supplementary Table 3.

Consistent with the literature about acute SARS-CoV-2 infection in the pediatric population[23], in our cohort, most children showed a mild-to-moderate clinical course, with 6 children (6.5%) presenting severe disease, only one of whom (1.1%) needed intensive care (Table 2). Children with underlying chronic conditions (i.e., genetic/metabolic conditions, hematological diseases, cardiological abnormalities, respiratory chronic disease, neurological disease, renal disease, severe obesity) accounted for about 25% of the entire population. Their clinical presentation in relation to SARS-CoV-2 infection did not significantly differ from the remaining cohort. The mean duration of hospitalization was 6 ± 5.7 days (Table 2). A secondary bacterial co-infection was diagnosed during hospitalization in 12 patients. Paracetamol ($n = 65$, 70.6%) and antibiotics ($n = 26$, 28.2%) were the most prescribed treatments. Glucocorticoids were administered in 4 children with COVID-19-related pneumonia.

Seven children fulfilling the criteria of MIS-C according to the Center for Disease Control and Prevention (CDC) criteria were enrolled. All patients presented positive SARS-CoV-2 serology at admission, and 3 of them also had a positive nasopharyngeal swab (Table 2). All patients presented with fever, and 6 (85.7%) had gastrointestinal symptoms, including vomiting ($n = 6$, 85.7%), diarrhea ($n = 4$, 57.1%) and abdominal pain ($n = 3$, 42.9%). Two patients (28.6%) developed severe myocarditis with impaired left-ventricular function and cardiac arrhythmias, and the other two (28.6%) underwent abdominal surgery. Intensive care support was needed in two cases (28.6%). All MIS-C patients received intravenous immunoglobulin and methylprednisolone boluses, and six (85.7%) received low-molecular-weight heparin. Two (28.6%) demonstrated a first-line treatment failure and were then treated with an IL-1 receptor antagonist, *Anakinra*. Compared to those with acute SARS-CoV-2 infection, children with MIS-C showed significantly longer hospitalization (Table 2).

Despite the severity of some clinical presentations, all patients improved significantly during hospitalization and were discharged at home.

Metabolomic signature discriminates children with SARS-CoV-2 infection from healthy controls

To define a metabolomic signature specific for pediatric COVID-19 patients, a PLS-DA analysis was performed on serum samples from 91 SARS-CoV-2 positive patients while admitted in the COVID-19 pediatric Unit in comparison to 41 healthy controls (Table 1 and Fig. 1). Gas chromatography-mass spectrometry (GC-MS) analysis of 139 serum samples (including T1, T2, T3 for SARS-CoV-2 infected patients and 41 controls, as indicated in Supplementary Table 3) allowed to detect 249 endogenous metabolites.

A clear separation between the metabolomic signature of controls (CTRL) and SARS-CoV-2 positive children was found, as highlighted in a

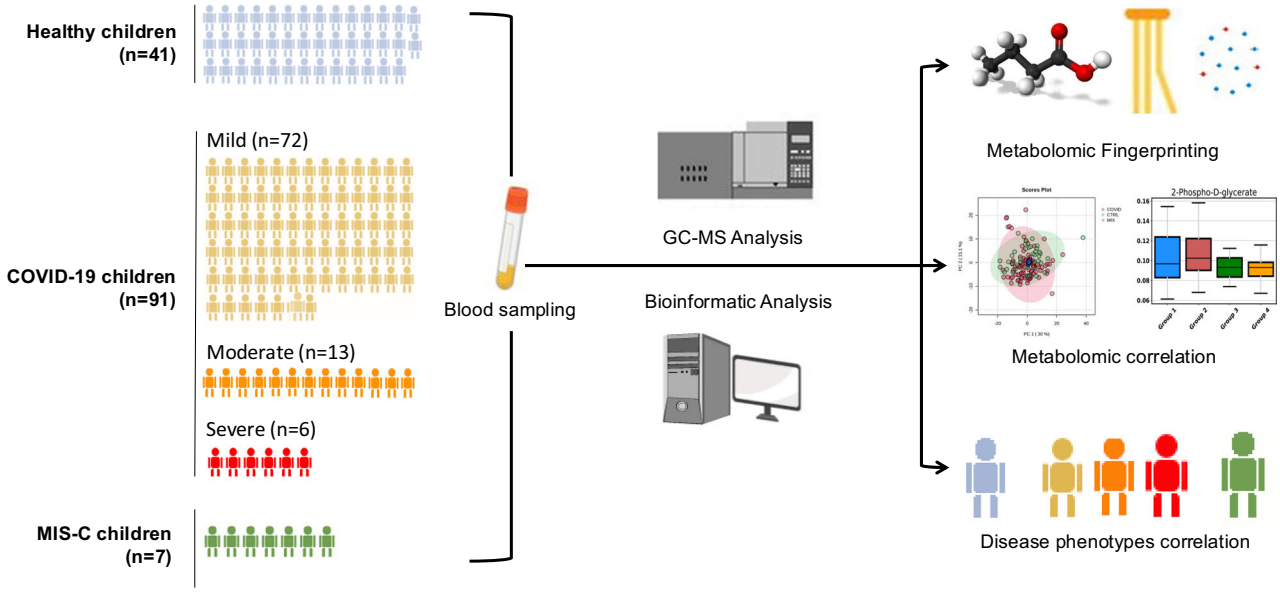

Fig. 1 | Study design. Overview of the study population, including children with acute SARS-CoV-2 infection (COVID-19 children, $n = 91$), children who fulfilled the criteria for MIS-C according to the Center for Disease Control definition (MIS-C children, $n = 7$) and controls (controls, $n = 41$). Serum samples were collected from COVID-19 and MIS-C children at different time points during the disease course, and only at admission from healthy controls. All serum samples were processed using the following workflow to obtain metabolomic data: metabolite extraction, gas chromatography-mass spectroscopy analysis (GC-MS), and bioinformatic analysis. Further computational analyses were used to identify specific metabolomic fingerprints of children with COVID-19 and MIS-C compared to controls, to define the main discriminant metabolic pathways, and correlate the metabolic pathways perturbations with patients' age, disease course and severity.

PLS-DA scatter plot (Fig. 2a). The best diagnostic performance of the PLS-DA classification model was achieved using four variables as the basis for classification (Fig. 2b). The permutation test statistically assessed the class separation of metabolomes by visually illustrating and measuring the statistical significance of COVID and CTRL metabolome separations and lack of overfittings (Fig. 2c). Performance indices based on 1000 permutations were: $p = 0.0045$ (9/2000) $R^2_Y = 0.753$, $Q^2_Y = 0.544$ (Fig. 2b, c). Seven metabolites, namely palmitic acid, 4-trimethyl-ammoniobutanoic acid, gluconic acid 1, sorbose, arabinose, glucose 3, 4-ketoglucose, showed a VIP-score higher than 2.0 (Fig. 2d), and are responsible for the PLS-DA observed distribution. Of those, Arabinose is the only one found to be upregulated in COVID-19 compared to controls, while the others are downregulated (Fig. 2d). Metabolite set enrichment analysis performed, including all differently expressed metabolites (Fig. 2e), allowed to identify lactose metabolism and glucose-alanine cycle as the top enriched pathways ($\log10\, p > 1$). Furthermore, as summarized in the metabolic systems map, interplaying sets involved in fatty acid metabolism are also enriched.

Age-dependent analysis of serum metabolomic profile reveals a distinct signature in patients above 3 years of age

Upon identification of a specific metabolome in pediatric COVID-19 patients, considering that the metabolomic profile varies across ages[24,25], we asked whether an age-dependent signature could be identified in our cohort. Given the wide age range of patients included in our population, and the related variability due to exposure to distinct metabolic drives, we investigated by GC-MS analysis the differences in the metabolomic profile across age groups, comparing children aged less than 2 months (mo), 2 mo to 3 years (yrs), 3–10 yrs and more than 10 yrs (Supplementary Fig. 2a).

No differences were found between patients younger than 2 mo and those between 2 mo and 3 yrs (Supplementary Fig. 2A), nor between patients aged 3–10 yrs vs those older than 10 yrs (Supplementary Fig. 2B). On the contrary, children with SARS-CoV-2 infection <3 yrs showed a distinct metabolomic profile compared to those >3 yrs of age (Supplementary Fig. 1C). To investigate whether this difference was disease specific or age-dependent, we first compared the metabolomic profile of healthy controls younger to those older than 3 yrs of age (Supplementary Fig. 2) and found that they also showed a distinct metabolic profile, as indicated by PLS-DA analysis, suggesting an age-dependent metabolomic signature also in controls. However, when we then compared COVID-19 patients to healthy controls by age groups, under 3 yrs of age we found no difference in the metabolomic serum profile (Fig. 3a–c), suggesting that the observed differences were mostly age-dependent rather than disease specific. On another hand, when comparing affected children >3 yrs of age to age-matched controls a distinct metabolomic signature was identified (Fig. 3d–f) with five metabolites showing a VIP-score higher than 2.0, namely arabinose 4, androstenedione, 2-hydroxy-phenylacetic acid glucuronide, 2-ethylexanoic acid and galactose1 (Fig. 3g). Metabolite set enrichment analysis performed including all differently expressed metabolites, identified lactose degradation, nucleotide sugars metabolism and androstenedione metabolism as the three-top enriched sets ($\log10\, p > 1$) (Fig. 3h). Altogether, these data indicate an age and disease-dependent metabolomic signature in COVID-19 affected children, that seems to also involve sexual hormonal pathways (Fig. 3h), while confirming the relevance of lactose and galactose metabolism.

Longitudinal analysis of serum metabolomic signature reveals significant variations over time during SARS-CoV-2 infection in children

We then investigated how the alterations in metabolic signature observed in acute COVID-19 changed over the disease course and whether they tended to normalize over time and resemble the profiles observed in controls. To this end, we conducted a longitudinal analysis of serum samples serially collected during hospitalization (T1-T2-T3) and at infection resolution (T4), when SARS-CoV-2 RNA was undetectable in respiratory samples (Supplementary Table 3), in comparison with HCs. Permutation statistics of the samples collected in different phases of SARS-CoV-2 infection demonstrated a clear separation of the metabolitic profiles of acute and symptomatic phases (T1-T2-T3), from those of the recovery phase (T4) and from HCs (Fig. 4a, $p = 0.039$ (78/2000) $R^2_Y = 0.414$, $Q^2_Y = 0.226$). The longitudinal analysis revealed an evolution of the metabolic fingerprint over time, with appreciable variations for some metabolites that showed a VIP-score higher than 2.0 (Fig. 4b), including arabinose 4, palmitic acid and sorbose. In line with what observed comparing affected children to controls

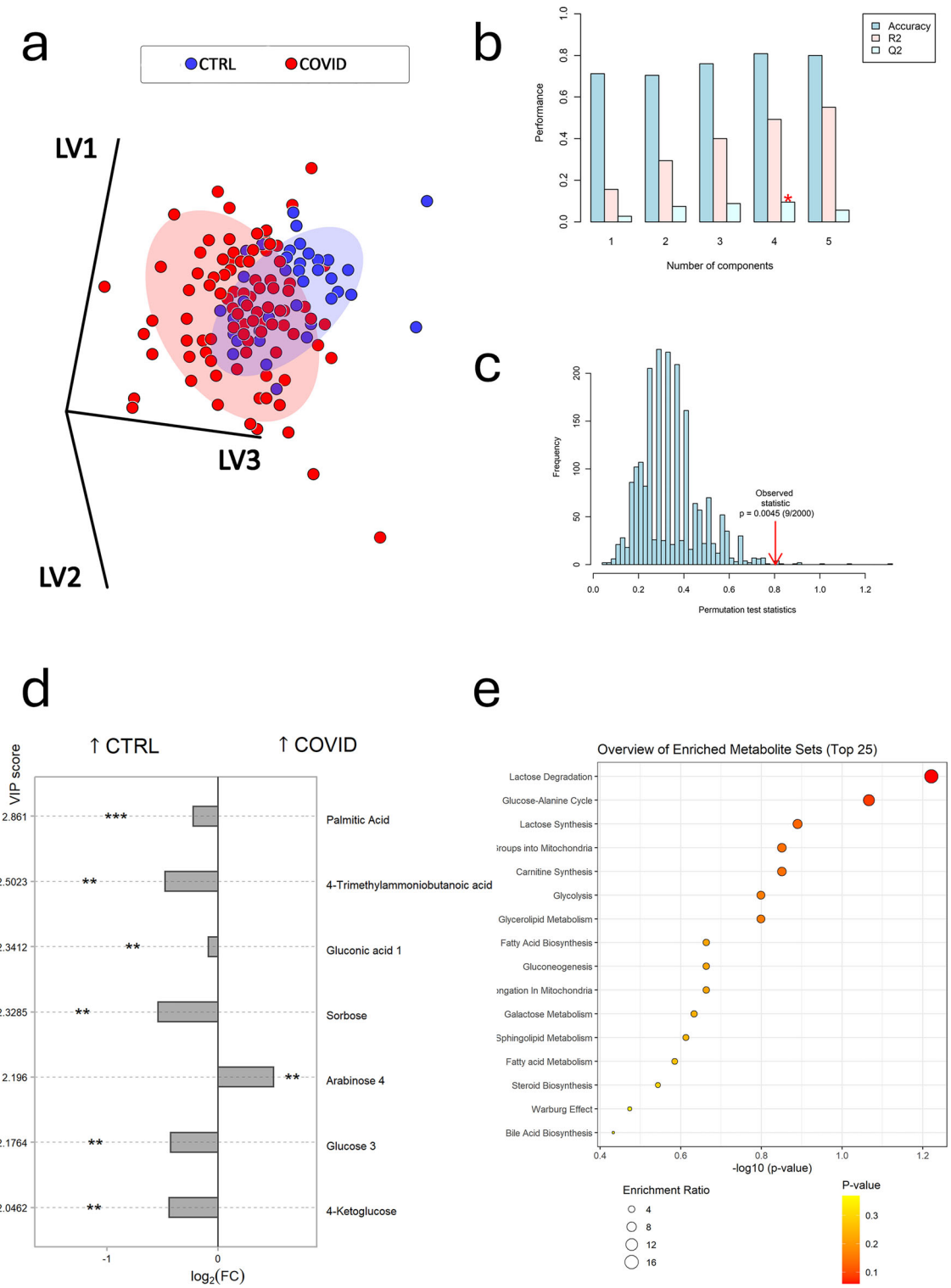

Fig. 2 | Serum metabolomic signature in children with SARS-CoV-2 infection compared to controls. a Partial least square-discriminant analysis (PLS-DA) classification model discerning healthy control subjects (CTRL, blue dots), from COVID-19 patients during the acute phase of infection (T1-T2-T3) (COVID, red dots). The explained variance of each latent variable (PC, principal component) is shown in brackets on the corresponding axis. **b** Diagnostic performance of the PLS-DA classification model when using different numbers of latent variable (number of components, x-axis). The best performance (denoted with a red star) is achieved when using four variables as the basis for classification. **c** PLS-DA model validation by permutation test based on separation distance. The two-sided *p*-value based on 1000 permutations is $p = 0.0045$. **d** The first 7 metabolites identified by the PLS-DA are reported. The number of variable importance in projection (VIP) was established by setting the VIP-score > 2.0. The increase or decrease in the serum level of single metabolites in COVID-19 patients and controls is reported as logarithmic fold change (log2FC). **e** Metabolite set enrichment analysis performed using the seven selected metabolites **d** identified lactose degradation and glucose-alanine cycle as the two metabolic pathways responsible for the discrimination between COVID-19 patients and controls. The circle dimension express the degree of enrichment ratio, and the color scale reflects the *p*-values (one-sided Fisher's exact test).

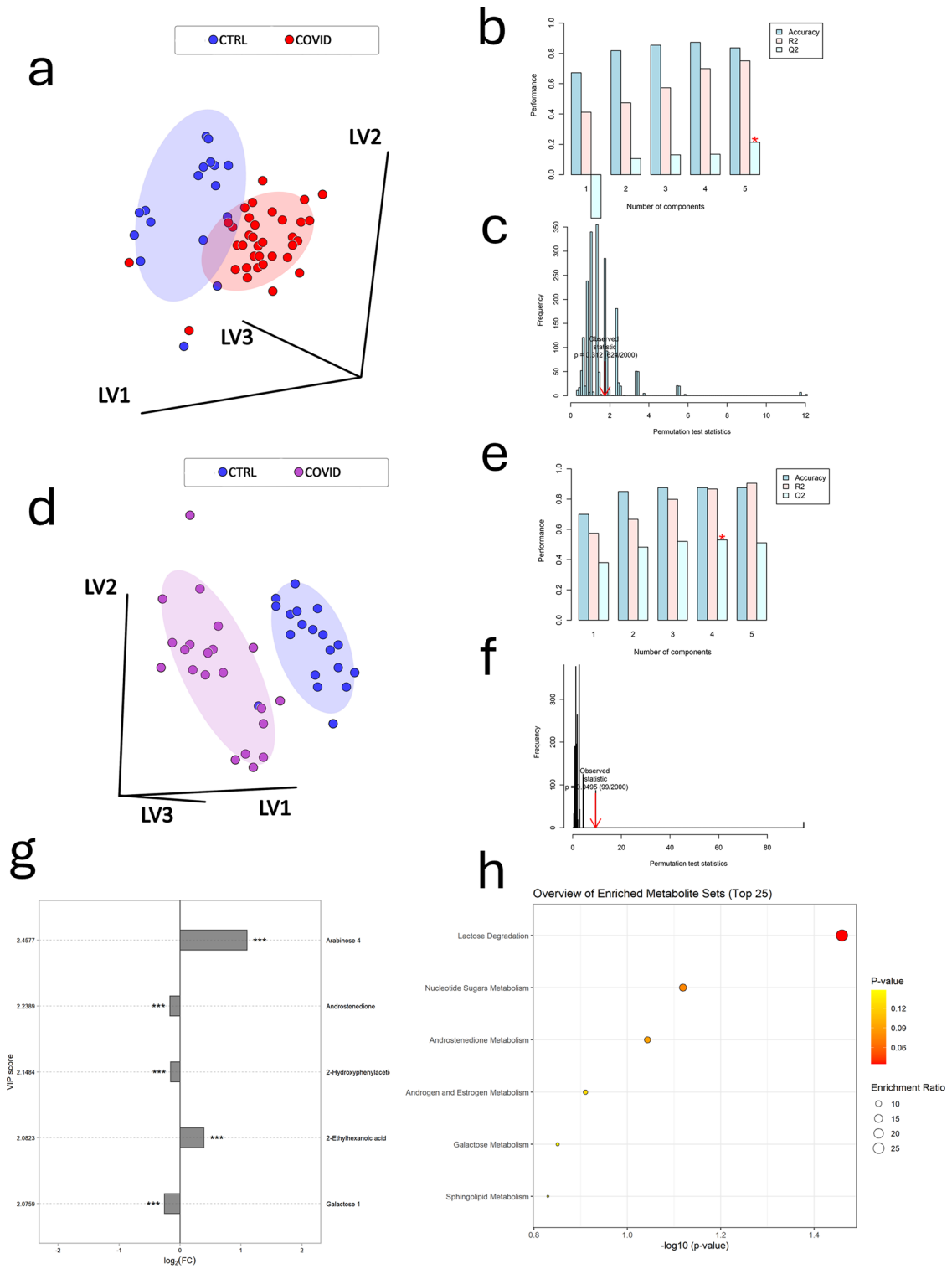

(Fig. 2e), the enrichment analysis revealed lactose metabolism and glucose-alanine cycle as the metabolic pathways most susceptible to variation over the course of SARS-CoV-2 infection (Fig. 4c). Thus, the pathways found altered in acute SARS-CoV-2 infection, especially in children above 3 years of age are subject to plastic changes over disease course.

The longitudinal evaluation revealed a clear trend toward increase for selected metabolites whose serum levels were low during the acute phase of the infection: those progressively increased to levels comparable to those detected in HCs, specifically palmitic acid, 4-trimethylammoniumbutanoic acid, hypoxanthine, glucose-3 and sorbose (Fig. 4d, e). A reverse trend was observed for arabinose-4 and talofuranose, two polysaccharides likely associated with SARS-CoV-2-related dysbiosis. Their serum levels resulted abundant in the early phase of the infection and gradually decreased to levels similar to HCs when SARS-CoV-2 was cleared from the host (Fig. 4d, e). The downregulation of hypoxanthine, found in the acute phase of SARS-CoV-2 infection (Fig. 4b), may be due to an enhanced activity of xanthine oxidase mediated by the hypoxic injury secondary to the SARS-CoV-2 infections, as reported for other viruses, including the respiratory syncytial virus (RSV).

All together, these findings revealed that the substantial changes in metabolic pathways that characterize the early phase of SARS-CoV-2

Fig. 3 | Age-dependent serum metabolomic signature in children with SARS-CoV-2 infection. a–c Partial least square-discriminant analysis (PLS-DA) classification model discerning healthy control subjects aged less than 3 years old (CTRL, blue dots), from COVID patients aged less than 3 years old during the acute phase (T1-T2-T3) (COVID, red dots). Diagnostic performance of the PLS-DA classification model, using different numbers of latent variables, denotes the best performance with 5 components as the basis for classification (marked with a red star). PLS-DA model validation by permutation test did not show statistically significant separation distance between COVID patients and controls (two-sided *p*-value based on 1000 permutations is $p = 0.312$, lower panels). **d–f** PLS-DA classification model is able to discern controls above 3 years of age (CTRL, blue dots) from COVID patients aged above 3 years of age during the acute phase (T1-T2-T3) (COVID, purple dots). The best diagnostic performance of PLS-DA (denoted with a red star) is achieved when using 4 components as the basis for classification. The model validation by permutation test based on separation distance showed a two-sided *p*-value of 0.048 based on 1000 permutations (lower panels). **g** The first 5 metabolites identified by the PLS-DA for patients aged above 3 years of age are reported. The number of variable importance in projection (VIP) was established by setting the VIP-score > 2.0. The increase or decrease in the serum level of single metabolites in COVID-19 patients and controls is reported as logarithmic fold change (log2FC). **h** Metabolite set enrichment analysis of PLS-DA for patients aged above 3 years identified Lactose degradation as the metabolic pathway mainly responsible for the discrimination between COVID-19 patients and controls. The circle dimension reflects the enrichment ratio, and the color scale the *p*-values (one-sided Fisher's exact test).

infection are transient and tend to restore upon SARS-CoV-2 clearance and clinical remission. The evidence of a restoration over the disease course further suggests that the identified metabolites are associated with the host-SARS-CoV-2 interaction.

Disease severity and systemic inflammation drive changes in metabolomic signature among pediatric COVID-19 patients

Perturbation of specific metabolic pathways has been described in adults with a severe course of SARS-CoV-2 infection[25]. On this basis, we investigated the association between metabolic pathways' alteration and severity of COVID-19 in children, to potentially identify specific metabolites associated with a severe presentation, a PLS-DA analysis was performed comparing the sera collected during the acute phase of infection (T1–T2) from children presenting with a severe ($n = 6$, 31 samples) or mild-to-moderate ($n = 85$, 98 samples) phenotype to those from HCs ($n = 41$).

Children with severe clinical presentations included those with interstitial pneumonia requiring specific treatment ($n = 4$), a child with acute encephalitis ($n = 1$) and another requiring intensive care due to severe sepsis-like presentation ($n = 1$). Only one patient needed intensive care, and none had a fatal outcome (Table 2).

Despite only a few children with severe clinical presentation were investigated, the PCA showed a clear segregation (Fig. 5a). The model was evaluated with cross validations $R^2_Y = 0.628$, $Q^2_Y = 0.319$ and permutation tests [$p < 5e\text{-}0.4$ (0/2000), not shown]. Thus, children with a more severe clinical phenotype showed a peculiar metabolic perturbation that differs from those with mild-to-moderate symptoms or from HCs. In a consistent pattern of change showing eighteen enriched metabolic sets, the metabolism of phenylacetate and purine were identified as the most commonly perturbed pathways (Fig. 5b).

Figure 5b illustrates the cross-sectional distribution of selected metabolites across healthy controls, mild COVID-19, and severe disease groups. Notably, some metabolites exhibit non-monotonic or biphasic patterns, such as stearic acid, which appears elevated in severe cases compared to both mild disease and controls. These patterns reflect the complex and dynamic nature of metabolic regulation, which may involve compensatory mechanisms rather than linear progression across disease severity.

The metabolites that best differentiated children with a severe rather than mild-to-moderate clinical presentation (VIP score > 2) were stearic and palmitic acid, hypoxanthine, arabinose and sorbose (Fig. 5c). Notably, sorbose, that was already demonstrated to be downregulated during the acute phase of SARS-CoV-2 infection with a gradual restoration overtime (Fig. 4c), showed an even more profound decrease in children presenting clinically compromised conditions.

The clinical spectrum of COVID-19 is a consequence of the variable immune responses to the virus. There is evidence that in subjects presenting with severe COVID-19 a dysfunctional host immune response, unable to inhibit viral replication and eliminate the infected cells, can lead to systemic inflammation, with increased serum levels of inflammatory markers (CRP, LDH, ferritin, procalcitonin, IL-6), endothelial injury (in some cases) and extensive tissue damage[25,26]. Albeit less common than in adults, this pro-inflammatory response can be triggered also in children with COVID-19. To characterize the metabolic perturbations associated with the inflammatory status, we decided to stratify our population of SARS-CoV-2-infected children based on the serum levels of inflammatory markers, such as CRP, procalcitonin (PCT) and interleukine-6 (IL-6) (Fig. 5 and Supplementary Fig. 4). Hence, we compared the metabolic signature of children showing serum CRP levels at admission higher than 100 mg/dl ($n = 2$), between 10 and 100 mg/dl ($n = 25$), 5 and 10 mg/dl ($n = 11$) or below 5 mg/dl ($n = 53$), and, similarly, those with levels of PCT higher than 5 ng/ml ($n = 1$), between 2 and 5 ng/ml ($n = 4$), 0.1 and 2 ng/ml ($n = 10$) or below 0.1 ng/ml ($n = 30$).

The PLS-DA showed a clear segregation pattern of COVID-19 patients in parallel with the degree of inflammation, either in the case of elevated CRP (Fig. 5d), permutation test statistics $p = 0.0025$ (5/2000) $R^2_Y = 0.629$, $Q^2_Y = 0.394$, or in those showing increased PCT (Fig. 5G) ($p = 0.001$ (2/2000), $R^2_Y = 0.641$, $Q^2_Y = 0.456$). A similar trend was observed when considering IL-6 serum levels (Supplementary Fig. 4A).

Selected metabolites are able to discriminate the inflammatory status of COVID-19 patients (Fig. 5e, h). Among those showing a VIP score higher than 2.0, some showed progressively increased levels in sera of children with high inflammatory markers, namely pyridinol, acetamide, pyrimidine, putrescine, benzylalcohol, and methylmaleic acid, talofuranose, benzoic acid (Fig. 5e, h). In contrast, stearic and palmitic acids demonstrated an inverse linear correlation with inflammation, showing decreased levels in children with the highest levels of inflammatory markers. Reduced circulating levels of palmitic acid, observed in our children with active disease as well as in those with elevated markers of inflammation, may reflect its consumption and internalization as a cell mediator of inflammation. A deeper dive in the fatty acid biosynthesis is included in Supplementary Fig. 5.

The enrichment analysis showed that the metabolism of glycerolipids is responsible for the main metabolic perturbations correlated with the inflammatory status based on CRP (Fig. 5f) and PCT (Fig. 5I) levels. In particular, we observed an increase in D-glycerate and glycerol levels in patients with moderate inflammation (looking at CRP levels, Supplementary Fig. 6). The metabolism of spermidine, a polyamine playing a pivotal role in cell internalization of viruses[27], was the only metabolic pathway able to discriminate patients with elevated CRP from those with elevated PCT.

All together these findings suggest that a severe clinical presentation, as well as the presence of systemic inflammation, as assessed by CRP and PCT, may be associated with appreciable changes in metabolomic signature.

MIS-C displays a distinct metabolomic profile compared to COVID-19 children

About 3–4 weeks after acute SARS-CoV-2 infection, a minority of children may develop an immune-mediated and typically severe disease characterized by hyperinflammation, endothelial disfunction, tissue damage, and multi-organ involvement. Previous evidence showed a significant increase in biomarkers related to type II IFN signaling, macrophage and neutrophil activation, endothelial injury and activation, matrisome-related inflammation, and septic shock in children with MIS-C[28]. We hypothesized that those children, whose clinical outcomes significantly differ from children with acute SARS-CoV-2 infection, may display a distinct metabolic profile compared to COVID-19 patients. Hence, we decided to characterize the perturbations of the serum metabolome of children with MIS-C ($n = 7$,

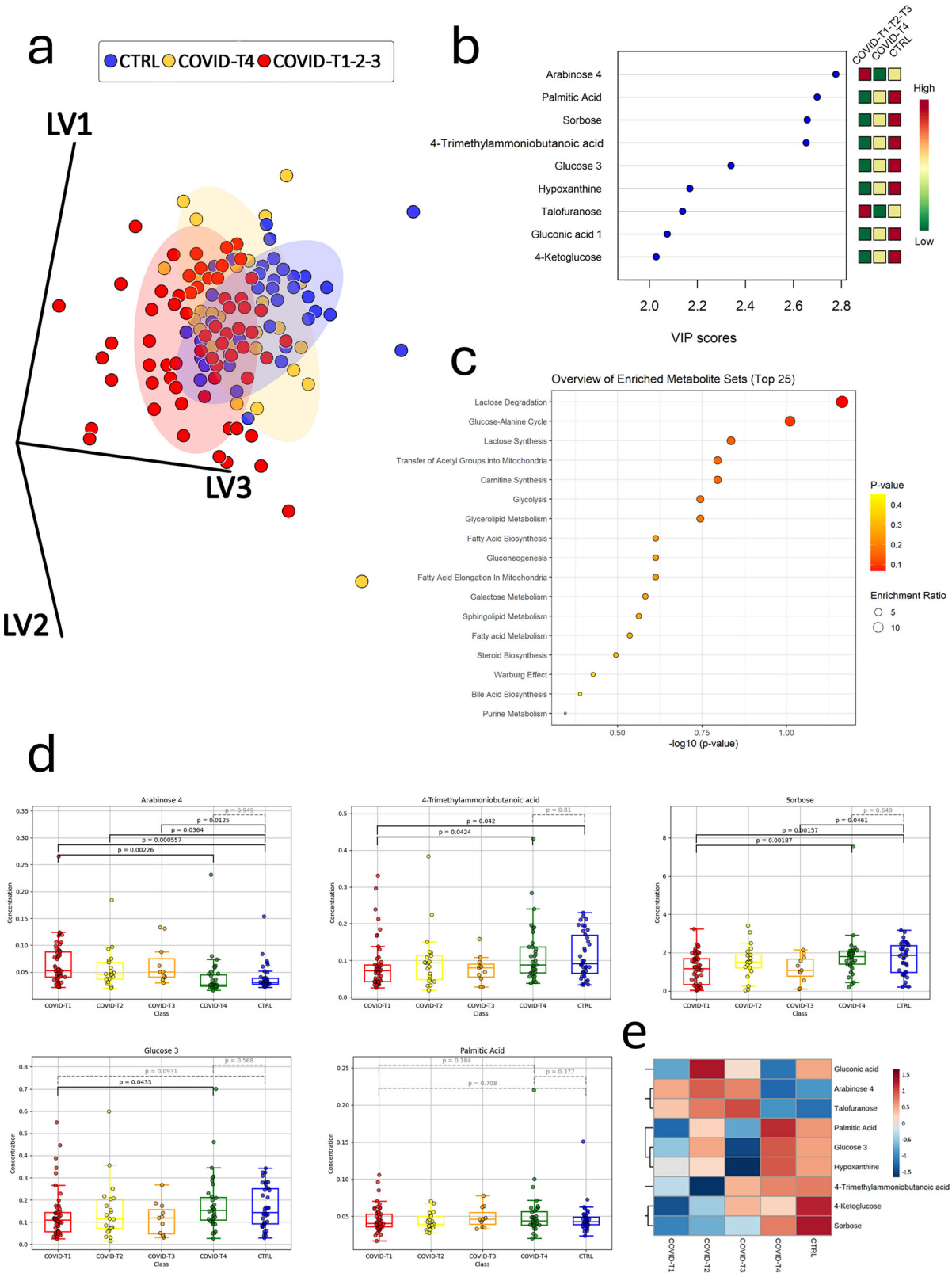

23 samples) during the acute and critical phase (T1 and T2) of the disease. All 7 (100%) patients showed positive antibodies against SARS-CoV-2 infection, and in 3 (42.8%) of them the viral nucleic acid was still detectable on nasopharyngeal specimens (Table 2).

Given the small sample size, to minimize the inter-personal variability, we compared the results of metabolomic analyses of MIS-C patient with those from a group of patients with acute SARS-CoV-2 infection ($n = 7$) as well as of HCs ($n = 7$), matched for age, sex and ethnicity in a 1:1 ratio.

Children fulfilling the criteria for MIS-C showed a higher degree of inflammation with elevated serum levels of CRP (mean 242.4 ± 126 mg/dl) and PCT (13.6 ± 7.8 ng/ml). The PLS-DA analysis of MIS-C samples obtained within 7 days of hospitalization, demonstrated a marked

Fig. 4 | Longitudinal evolution of selected serum metabolites during COVID-19 infection and comparison with healthy controls. a Partial least square-discriminant analysis (PLS-DA) classification model discerning control subjects (CTRL, blue dots), from COVID-19 patients during the acute phase of infection (T1-T2-T3) (red dots) and after the first negative nasopharyngeal swab (yellow dots). The explained variance of each variable (PC) is shown in brackets on the corresponding axis. **b** The first 9 metabolites identified by the PLS-DA are reported. The number of variable importance in projection (VIP) was established by setting the VIP-score > 2.0. The increase or decrease in the serum level of single metabolites in COVID-19 patients and controls is reported as logarithmic fold change (log2FC). The color of the squares on the right indicate the relative amount of the corresponding metabolite in each study group (red, high, yellow, intermediate, green, and low). **c** Metabolite set enrichment analysis performed using the selected metabolites identified lactose degradation and glucose-alanine cycle as the two main differentially enriched metabolic pathways. The circle dimension reflects the enrichment ratio, and the color scale the *p*-values (one-sided Fisher's exact test). **d** To specifically study the variations of metabolic signature during different phases of SARS-CoV-2 infection, the serum concentration of specific metabolites (with VIP score > 2) was evaluated in clinical samples collected at different times. Boxplots showing the concentration levels of five representative metabolites (arabinose 4, palmitic acid, glucose 3, sorbose, and 4-trimethylammoniobutanoic acid) across the four disease timepoints in COVID-19 pediatric patients—T1 (hospital admission, red), T2 (hyperacute phase, yellow), T3 (discharge, orange), T4 (follow-up, green)—and healthy controls (CTRL, blue). For each metabolite, horizontal bars indicate pairwise comparisons. ANOVA two-sided *p*-values are displayed for all comparisons: in gray, we highlight comparisons between T1 vs. T4 and T1 vs. CTRL, which reflect both longitudinal changes and divergence from baseline physiology. In black, only statistically significant comparisons ($p < 0.05$) are shown. Data are presented as median (continuous line), 95% confidence intervals (box), and ranges (vertical line), and significance was calculated using appropriate nonparametric tests adjusted for multiple comparisons. **e** Heatmap visualization and clustering analysis of the normalized abundance of the top 10 discriminatory metabolites (selected by VIP > 2.0 from PLS-DA), comparing the four COVID timepoints (T1–T4) with healthy controls (CTRL). Metabolites are hierarchically clustered by Euclidean distance. The color scale expresses the fold change (increase, red; decrease, blue).

perturbation of the metabolic profile ($p = 0.0045$ 9/2000, $R^2_Y = 0.817$, $Q^2_Y = 0.452$), completely distinct from children with acute SARS-CoV-2 infection (Fig. 6a). We identified ten metabolites responsible for the differences between the groups (VIP score > 1.5): urobilin, hydroquinone, isobutanol, 2,3-dihydroxbutanoic acid, xylopyranose, mevalonic acid, quininic acid, inosine, methionine, pyrogallol. All these metabolites resulted significantly upregulated during the hyper-acute phase of MIS-C compared to children with acute SARS-CoV-2 infection and HCs (Fig. 6b). In those patients, the projection of metabolic enrichment demonstrated a perturbation of the metabolism of glycerophosphate shuttle, the biosynthesis of spermidine and spermine, the metabolism of riboflavin and glycerolipids (Fig. 6c), similarly to children showing high degree of inflammation during acute COVID-19 (Fig. 5e, h).

We identified a metabolic fingerprint distinctive of children in the early and hyper-acute phase of MIS-C. Their metabolic profile differs from healthy children and appears to be qualitatively different from children with acute SARS-CoV-2 infection. These findings may help identify early and reliable biomarkers able to discriminate children with acute COVID-19 from those with MIS-C, that are usually candidates to a different management.

Discussion

Serum metabolomic profile in children with COVID-19 or MIS-C has been poorly studied, in contrast to the evidence available for adult COVID-19 patients. To address this gap, we performed the first pediatric longitudinal study aiming at defining the serum metabolomic profile across different age groups and in relation with clinical outcomes and immunological severity biomarkers.

Comparing 91 SARS-CoV-2 positive children admitted to our University hospital to 41 age and sex matched noninfected controls, we delineated a disease-specific metabolomic signature that includes lactose metabolism, glucose-alanine cycle, and fatty acid metabolism, as top-enriched pathways. Among the top 25 enriched pathways we also found sphingolipid metabolism, that is interconnected with fatty acid oxidation and lipogenesis. Furthermore, we identified an age-dependent and disease-specific signature in COVID-19 children above three years of age featuring sexual hormonal pathways in addition to glucose metabolism. Those metabolic perturbations were fully restored upon viral clearance and clinical remission, suggesting that, in children, SARS-CoV-2 has a transient impact on the metabolic profile of the host. Lastly, we found a significant perturbation in lipid metabolism associated with COVID-19-related inflammatory response and clinical severity. Notably, despite the most enriched pathways were similar to those of severe COVID-19, MIS-C patients displayed a unique signature featuring specific metabolites that might be considered in the future for validation in early identification of MIS-c cases.

So far, only a few papers explored the metabolic perturbations occurring in SARS-CoV-2 infected children. Wang et al. described a multi-omic approach in a small pediatric cohort revealing that SARS-CoV-2 infection in children is linked to both deteriorative immune responses and protective antioxidant/ anti-inflammatory processes. Among the identified metabolites, metilmalonic acid and mannitol were hypothesized to play a role in suppressing coronaviral replication. In line with this work, we identified a role for central metabolism, such as glycolysis, and several pathways involving aminoacidic metabolism. However, we also found a major enrichment in lipid and fatty acid metabolism that was not reported in the former study. Some of those pathways can be ascribed to the so-called Warburg effect that refers to a viral metabolic reprogramming in infected cells featuring increased glycolytic pathways to supply reducing equivalents and precursors for macromolecule biosynthesis, along with nucleotide and lipid biosynthesis, also enhanced in biological processes associated with rapid cell proliferation, including viral infections[7]. The differences observed between these studies might be due to distinct methodologies, but also to a lower sample size and lack of severe COVID cases in the work by Wang et al.[13].

In contrast to SARS-CoV-2, RSV, frequent viral agent in the first year of life, enhances production of xanthosine, phosphoserine N-acetyl neuraminate metabolites while downregulating N-acetylglucosamine, glycerol-3-phosphate, a-ketoglutarate, CMP N-acetyl-neuraminate in the sera of infected compared to healthy children[29] Altogether those evidences suggest that, despite a shared metabolomic signature in response to acute infections (i.e. Warburg effect), each respiratory virus promotes a distinct metabolomic fingerprint. On another hand, children with recurrent respiratory infections featured alterations of bile acids, steroid hormones and succinic acid metabolism, suggesting that chronic respiratory infections may impact serum metabolome in a further different fashion[30].

Metabolomic data obtained from children vaccinated against SARS-CoV-2 with an inactivated virus also revealed a significant impact of the infection on amino acid metabolism. However, the pathways affected by vaccination and natural infection were different, the latter mainly impacting arginine biosynthesis, alanine, aspartate and glutamate metabolism[31].

Importantly, age, gender and growth and the related hormonal status may also influence the metabolome[32–35]. As a consequence, the metabolic status in children is different from those observed in adults, in relation to the changing physiology[36]. That is why results obtained in adult patients should be cautiously extrapolated onto the pediatric population.

Previous studies performed in adult COVID-19 patients revealed a crucial role for amino acid metabolism[37], with tryptophan, threonine, glutamate, and kynurenine being correlated with viral load[38]. A downregulation of lipid pathways, including fatty acids and sphingolipids, and an upregulation of steroid hormonal pathways have also been found in adults with severe COVID-19[6].

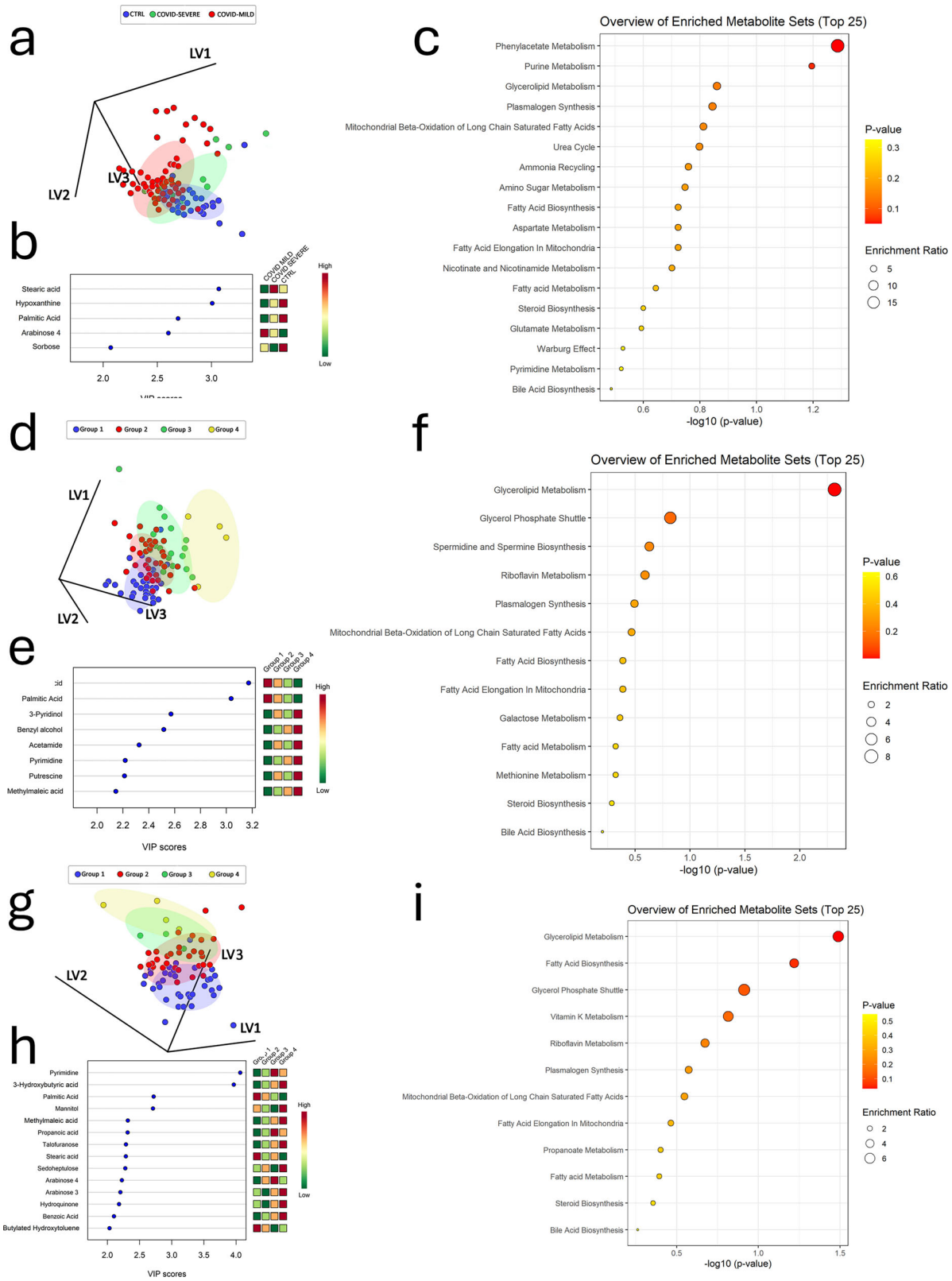

Since our pediatric population was distributed across a wide age range, to dissect the age-related differences across children with SARS-CoV-2 infection, we compared the metabolomic signature across age groups within COVID-19 pediatric patients, and the only difference was found when comparing COVID-19 children below and above three years of age. Notably, an age-dependent signature was also identified in controls below and above 3 years, indicating that age might be an important driver of some of the observed age differences. To test this hypothesis, we compared COVID-19 kids and age-matched controls by age groups and observed that while their metabolomic signature was not different between patients and controls below three years of age, older COVID-19 children displayed a distinct metabolomic signature compared to age-matched controls,

Fig. 5 | Metabolomic signature in relation with clinical and biochemical severity of SARs-CoV-2 infection in children. a Partial least square-discriminant analysis (PLS-DA) classification model discerning healthy controls (CTRL, blue dots), from COVID-19 patients with either a mild (red dots) or a severe (green dots) clinical presentation. The explained variance of each component is shown in brackets on the corresponding axis. **b** The first 5 metabolites identified by the PLS-DA are reported. The number of variable importance in projection (VIP) was established by setting the VIP-score > 2.0. The colored squares on the right indicate the relative amount of the corresponding metabolite in each study group. **c** Metabolite set enrichment analysis performed using the selected metabolites, identified phenylacetate and purine metabolism as the top metabolic pathways differentially enriched in the three groups. The marker dimension express enrichment ratio, and the color scale expresses the *p*-values (one-sided Fisher's exact test). Similar analysis was performed between healthy controls (blue dots) and COVID-19 patients with different degree of inflammation as defined by two inflammatory markers: C-reactive protein (CRP) (**d**–**f**) and procalcitonin (PCT) (**g**–**i**). **d**, **g** report the results of the PLS-DA that clearly discriminate the healthy control subjects from children with acute SARS-CoV-2 infection were classified in three different groups based on the serum level of C-reactive protein (group 2, red: CRP value 5–10 mg/L, group 3, green: CRP value 10–100 mg/L, group 4, yellow: CRP > 100 mg/L) or procalcitonin (group 2, red: PCT value 0.1–1 ng/mL, group 3, green: PCT value 1.1–5 ng/mL, group 4, yellow: PCT value > 5 ng/mL). The explained variance of each component is shown in brackets on the corresponding axis. Reports the first 8 and 14 metabolites identified by the PLS-DA with VIP-score > 2.0 for children showing high inflammatory markers, CRP (**e**) and PCT (**h**), respectively. In all cases, the colored squares on the right indicate the relative amount of the corresponding metabolite in each study group. Among the top 25 metabolite sets included in the enrichment analysis, glycerolipid metabolism was identified as the top differentially enriched metabolic pathway between healthy controls and COVID-19 patients with different degrees of inflammation. The circle size express enrichment ratio, and the color scale reflects the *p*-values (one-sided Fisher's exact test).

featuring lactose degradation, nucleotide sugars metabolism and androstenedione metabolism. This evidence suggested that while age was the main driver of the observed metabolomic differences in younger kids, a disease-specific signature was identified in older children that also involves sexual hormones. This does not seem to be related to a significantly different representation of males and females in controls compared to COVID-19 patients. Yet, further differences between females and males have not been investigated in our dataset.

To test whether the observed differences were transient and restored over time, in parallel with the clinical resolution of the disease, we performed a longitudinal analysis of a subset of COVID-19 patients followed up until SARS-CoV-2 clearance, that revealed lactose metabolism and glucose-alanine cycle as the two metabolic pathways more susceptible to variation over the disease course. In particular, our data pointed to a downregulation of palmitic acid, 4-ketoglucose, glucose-3, sorbose and 4-trimethylammoniumbutanoic acid levels in the acute inflammatory phase of the disease, with a gradual restoration to higher levels, similar to those observed in non-COVID-19 controls, upon clearance of the virus. Suggesting a shift towards lactose metabolism, glycolysis and glucose-alanine cycle in the acute phase of the disease. The downregulation of hypoxanthine in the acute phase of SARS-CoV-2 infection, may be due to an enhanced activity of xanthine oxidase mediated by the hypoxic injury secondary to the SARS-CoV-2 infections, as reported for other viruses, including the RSV[39]. On the contrary, our data revealed an upregulation of arabinose-4 and talofuranose in the acute phase and a gradual normalization to levels comparable to those observed in controls upon viral clearance. This seems to point to a possible involvement on SARS-CoV-2-related dysbiosis in fact arabinose may derive from intestinal epithelial cells[40].

Altogether, these findings reveal that the substantial changes in metabolic pathways that characterize the early phase of SARS-CoV-2 infection are transient and tend to restore upon SARS-CoV-2 clearance and clinical remission. The evidence of a restoration of the observed metabolic changes over the disease course further supports the concept that the identified fingerprints are related to the host-virus interactions and possibly COVID-19 pathogenesis.

As a matter of fact, environmental factors, including diet, can promote further alterations in the metabolic profile[33,34,41,42]. In our study, all COVID-19 patients in the same age group consumed a comparable diet during hospitalization (including collection time points T1, 2, and 3), indicating that the intra-individual metabolomic differences observed between T1–2–3 have not been influenced by dietary variations. In contrast, we could not control for dietary intake pre-admission nor at follow-up appointment (T4 samples) while patients were not hospitalized as well as for the control group. This represents a limitation of our study, in fact we cannot exclude that the heterogeneity of dietary composition might have partly contributed to the observed metabolomic changes. Nevertheless, the wide variability within controls and remission samples (T4) indicate that interindividual variations should not be the main drivers of the observed changes in COVID-19 patients compared to controls.

Then we investigated whether a distinct metabolic profile could be associated with either clinical or biochemical disease severity and found a perturbation in phenylacetate and purine metabolism pathways when comparing distinct severity groups. Phenylacetate metabolism plays a key role in nitrogen excretion and bacterial metabolism[43] while purine metabolism is often implicated in biological processes with high cell turnover and has the purpose to maintain optimal levels of nucleotides in the tissues[44]. Of note, a decrease in sorbose, while an increase of stearic acid was observed in children with a severe clinical presentation, suggesting not only a role for sugar but also for fatty acid metabolism in children with severe COVID-19.

Looking at the differences across COVID-19 patients in the metabolomic profile in relation with the serum levels of inflammatory markers (including CRP and PCT), our data revealed that the main perturbed pathway was glycerolipid metabolism, known to be involved also in other infectious[45,46] as well as in chronic inflammatory and metabolic conditions[47,48]. The metabolism of spermidine, a polyamine playing a pivotal role in viral internalization and autophagy[49], was also perturbed in relation with changes in CRP levels. A similar increase in the spermidine pathways were also found in adult patients with severe COVID-19[50].

Selected metabolites, including stearic and palmitic acids, demonstrated an inverse correlation with inflammation, showing decreased levels in children with the highest levels of inflammatory markers. Palmitic acid induces inflammatory response through different pathways, including Toll-like receptor agonism (i.e., TLR-4), production of chemokines and macrophage activation, stimulation of IL-1β, and activation of the inflammasome[51]. Reduced circulating levels of palmitic acid, observed in our children with active disease as well as in those with elevated markers of inflammation, may reflect its consumption as a cell mediator of inflammation. Selected metabolites showing a VIP score higher than 2.0 showed progressively increased levels in sera of children with high inflammatory markers, namely pyridinol, acetamide, pyrimidine, putrescine, benzylalcohol, and methylmaleic acid, talofuranose, benzoic acid. Independently from the variations of individual metabolites, overall our findings suggest that a severe clinical presentation as well as the presence of systemic inflammation, may be associated with appreciable and similar changes in metabolomic signature.

Finally, this study provides the first comparative analysis of the serum metabolic signature of COVID-19 vs MIS-C children hospitalized and followed up over time. MIS-C children displayed a perturbation of the metabolism of glycerophosphate shuttle, the biosynthesis of spermidine and spermine, the metabolism of riboflavin and glicerolipids, similarly to what observed in children with high levels of inflammatory markers during acute COVID-19, even though the PLS-DA analysis of MIS-C samples showed a distinct signature compared to those of children with acute SARS-CoV-2 infection, including urobilin, hydroquinone, isobutanol, 2,3-dihydroxbutanoic acid, xylopyranose.

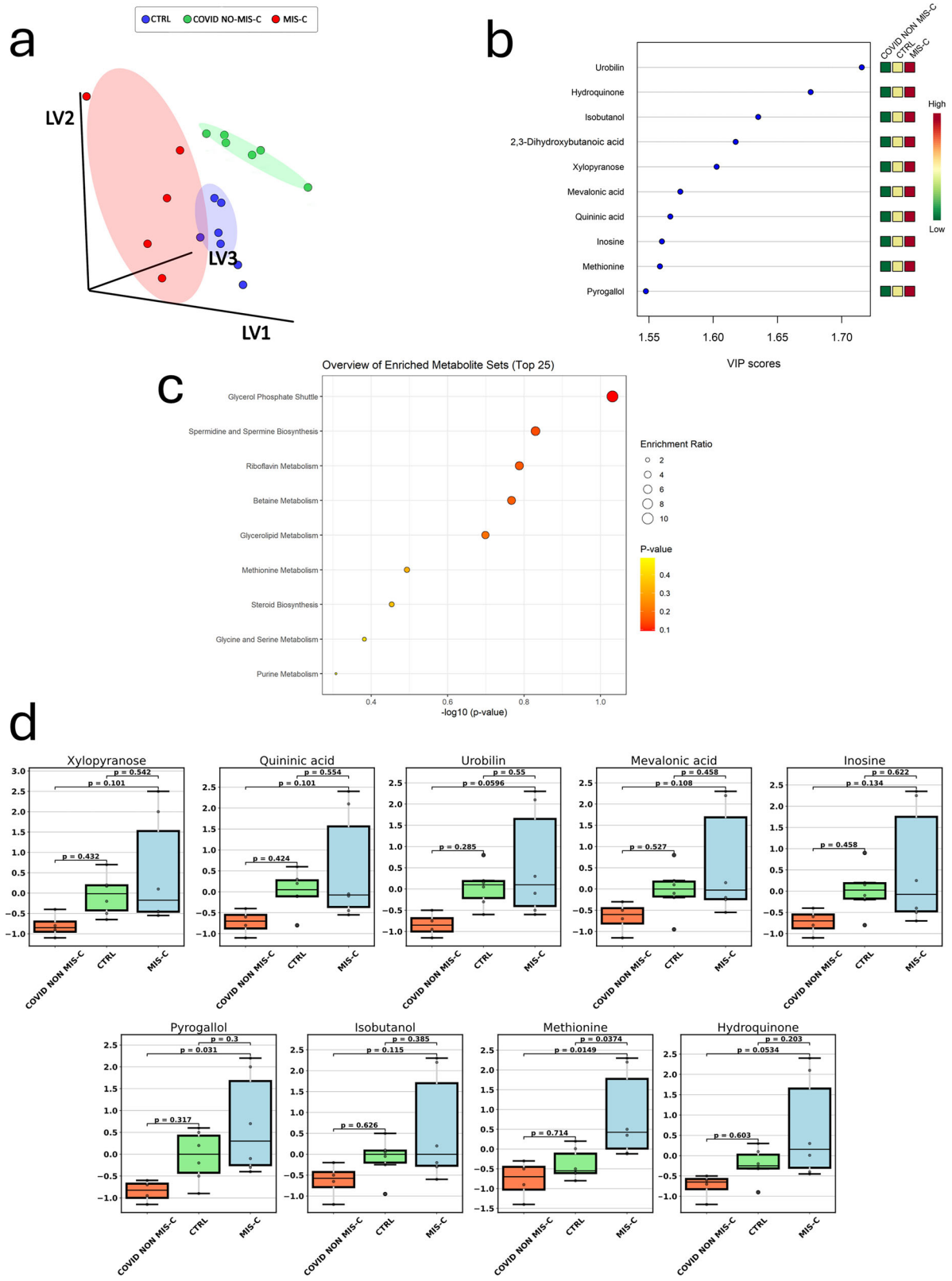

Despite the low number of MIS-C patients does not allow to make definite conclusions about the observed differences and their biological relevance, our study delineates an original metabolic fingerprint distinctive of children in the early and hyper-acute phase of MIS-C that profoundly differs from healthy children, but also from children with acute SARS-CoV-2 infection.

The study design did not allow to define prognostic markers; however, our data will hopefully serve as a base to design further studies that will be able to test whether any of the identified metabolites may serve as a prognostic marker for severity or MIS-C development. Another limitation of the study is related to the lack of stratification of the enrolled patients based on the different treatment received during hospitalization, that might impact

Fig. 6 | Distinct metabolomic signature in MIS-C patients compared with SARS-CoV-2 pediatric patients and controls. a Partial least square-discriminant analysis (PLS-DA) classification model discerning healthy controls (CTRL, blue dots), from COVID-19 patients during the acute phase of infection (T1–T2) (red dots) and MIS-C patients during the critical phase (green dots). Patients were age and sex-matched 1:1:1, $X = 21$ biological independent samples. The explained variance of each component is shown in brackets on the corresponding axis. **b** The first 10 metabolites identified by the PLS-DA are reported. The number of variable importance in projection (VIP) was established by setting the VIP-score > 2.0. In all cases, the colored squares on the right indicate the relative amount of the corresponding metabolite in each study group. **c** Metabolite set enrichment analysis performed using the selected metabolites identified glucose-phosphate shuttle and spermidine/spermine biosynthesis as the two top differential enriched metabolic pathways between the three groups. The circle size reflects the enrichment ratio, and the color scale the *p*-values (one-sided Fisher's exact test) (**d**) abundance of single metabolites in children with MIS-C, acute COVID-19 (non-MIS-C) and healthy controls. The abundance of individual metabolites is depicted as the median (continuous line), along with 95% confidence intervals (box) and ranges (vertical line).

the metabolic signature. However, patients with MIS-C were enrolled prior to any anti-inflammatory treatment, thus eliminating a potential confounding factor. Finally, we are referencing a time frame during which ancestral SARS-CoV-2 and B.1.1 variants (alpha, Spanish) or, in a minority of cases, B.1 variants (beta, delta) were prevalent. Therefore, our data does not pertain to the variants stemming from Omicron.

In conclusion, our study provides the first longitudinal analysis of metabolomic perturbation occurring in SARS-CoV-2 infected children, revealing their variations across age groups, disease course, clinical severity and degree of systemic inflammation. Our results shed light on the age-dependent metabolic fingerprint in COVID-19, on the transient nature of most of the observed perturbations and on their relation with systemic inflammation related to the host-viral interaction.

Data availability

The datasets generated and analysed during the current study are included in this published article as Supplementary data files. Source data for Figures from 1 to 6 can be accessed in Supplementary Data 1. A complete serum metabolic dataset from the current study is not stored in any public repository, yet it may be available from the corresponding author on reasonable request.

Received: 19 August 2024; Accepted: 3 February 2026;
Published online: 27 February 2026

References

1. Ludvigsson, J. F. Systematic review of COVID-19 in children shows milder cases and a better prognosis than adults. *Acta Paediatr.* **109**, 1088–1095 (2020).
2. Girona-Alarcon, M. et al. The different manifestations of COVID-19 in adults and children: a cohort study in an intensive care unit. *BMC Infect. Dis.* **21**, 87 (2021).
3. Garazzino, S. et al. Epidemiology, clinical features and prognostic factors of pediatric SARS-CoV-2 infection: results from an Italian multicenter study. *Front. Pediatr.* **9**, 649358 (2021).
4. Rhedin, S. et al. Risk factors for multisystem inflammatory syndrome in children-a population-based cohort study of over 2 million children. *Lancet Reg. Health Eur.* **19**, 100443 (2022).
5. Stephenson, T. et al. Physical and mental health 3 months after SARS-CoV-2 infection (long COVID) among adolescents in England (CLoCk): a national matched cohort study. *Lancet Child Adolesc. Health* **6**, 230–239 (2022).
6. Shen, B. et al. Proteomic and metabolomic characterization of COVID-19 patient sera. *Cell* **182**, 59–72 (2020).
7. Thaker, S. K., Ch'ng, J. & Christofk, H. R. Viral hijacking of cellular metabolism. *BMC Biol.* **17**, 59 (2019).
8. Allen, C. N. S., Arjona, S. P., Santerre, M. & Sawaya, B. E. Hallmarks of metabolic reprogramming and their role in viral pathogenesis. *Viruses* **14**, 602 (2022).
9. Hoxha, M. What about COVID-19 and arachidonic acid pathway? *Eur. J. Clin. Pharm.* **76**, 1501–1504 (2020).
10. Blasco, H. et al. The specific metabolome profiling of patients infected by SARS-COV-2 supports the key role of tryptophan-nicotinamide pathway and cytosine metabolism. *Sci. Rep.* **10**, 16824 (2020).
11. San Juan, I. et al. Abnormal concentration of porphyrins in serum from COVID-19 patients. *Br. J. Haematol.* **190**, e265–e267 (2020).
12. Pang, Z., Chong, J., Li, S. & Xia, J. MetaboAnalystR 3.0: toward an optimized workflow for global metabolomics. *Metabolites* **10**, 186 (2020).
13. Wang, C. et al. Multi-omic profiling of plasma reveals molecular alterations in children with COVID-19. *Theranostics* **11**, 8008–8026 (2021).
14. Centers for Disease Control and Prevention. Emergency Preparedness and Response: Multisystem Inflammatory Syndrome in Children (MIS-C) Associated with Coronavirus Disease 2019 (COVID-19) https://emergency.cdc.gov/han/2020/han00432.asp (2020).
15. Troisi, J. et al. Metabolomic signature of endometrial cancer. *J. Proteome Res.* **17**, 804–812 (2018).
16. Wold, S., Sjöström, M. & Eriksson, L. Partial least squares projections to latent structures (PLS) in chemistry. in (eds von Ragué Schleyer, P. et al.) *Encyclopedia of Computational Chemistry* (John & Wiley Sons, 1998).
17. Sysi-Aho, M. et al. Normalization method for metabolomics data using optimal selection of multiple internal standards. *BMC Bioinform.* **8**, 93 (2007).
18. Kuhn, M. Building predictive models in R using the caret package. *J. Stat. Softw.* **28**, 1–26 (2008).
19. Szymańska, E., Saccenti, E., Smilde, A. K. & Westerhuis, J. A. Double-check: validation of diagnostic statistics for PLS-DA models in metabolomics studies. *Metabolomics* **8**, 3–16 (2012).
20. Domingos, P. MetaCost: a general method for making classifiers cost-sensitive. In *Proc. Fifth ACM SIGKDD International Conference Knowledge Discovery and Data Mining* 155–164 (ACM, 1999).
21. Sumner, L. W. et al. Proposed minimum reporting standards for chemical analysis chemical analysis working group (CAWG) metabolomics standards initiative (MSI). *Metabolomics* **3**, 211–221 (2007).
22. Xia, J. & Wishart, D. S. MetPA: a web-based metabolomics tool for pathway analysis and visualization. *Bioinformatics* **26**, 2342–2344 (2010).
23. Pellegrino, R., Chiappini, E., Licari, A., Galli, L. & Marseglia, G. L. Prevalence and clinical presentation of long COVID in children: a systematic review. *Eur. J. Pediatr.* **181**, 3995–4009 (2022).
24. Chiu, C. Y. et al. Metabolomics reveals dynamic metabolic changes associated with age in early childhood. *PLoS ONE* **11**, e0149823 (2016).
25. Pang, Z., Zhou, G., Chong, J. & Xia, J. Comprehensive meta-analysis of COVID-19 global metabolomics datasets. *Metabolites* **11**, 44 (2021).
26. García, L. F. Immune response, inflammation, and the clinical spectrum of COVID-19. *Front. Immunol.* **11**, 1441 (2020).
27. Firpo, M. R. et al. Targeting polyamines inhibits coronavirus infection by reducing cellular attachment and entry. *ACS Infect. Dis.* **7**, 1423–1432 (2021).
28. Sacco, K. et al. Immunopathological signatures in multisystem inflammatory syndrome in children and pediatric COVID-19. *Nat. Med.* **28**, 1050–1062 (2022).
29. Teoh, S. T. et al. Combined plasma and urinary metabolomics uncover metabolic perturbations associated with severe respiratory syncytial

viral infection and future development of asthma in infant patients. *Metabolites* **12**, 178 (2022).
30. Bozzetto, S. et al. Metabolomic profile of children with recurrent respiratory infections. *Pharm. Res.* **115**, 162–167 (2017).
31. Wang, Y. et al. Blood transcriptome responses in patients correlate with severity of COVID-19 disease. *Front. Immunol.* **13**, 1043219 (2023).
32. Nagao-Kitamoto, H. & Kamada, N. Host-microbial cross-talk in inflammatory bowel disease. *Immune Netw.* **17**, 1–12 (2017).
33. Storr, M., Vogel, H. J. & Schicho, R. Metabolomics: is it useful for inflammatory bowel diseases? *Curr. Opin. Gastroenterol.* **29**, 378–383 (2013).
34. Lin, H. M., Helsby, N. A., Rowan, D. D. & Ferguson, L. R. Using metabolomic analysis to understand inflammatory bowel diseases. *Inflamm. Bowel Dis.* **17**, 1021–1029 (2011).
35. Sperisen, P., Cominetti, O. & Martin, F. P. Longitudinal omics modeling and integration in clinical metabonomics research: challenges in childhood metabolic health research. *Front. Mol. Biosci.* **2**, 44 (2015).
36. Carroll, M. W. et al. The impact of inflammatory bowel disease in Canada 2018: children and adolescents with IBD. *J. Can. Assoc. Gastroenterol.* **2**, S49–S67 (2019).
37. Sindelar, M. et al. Longitudinal metabolomics of human plasma reveals prognostic markers of COVID-19 disease severity. *Cell Rep. Med.* **2**, 100369 (2021).
38. Maeda, R. et al. Amino acid catabolite markers for early prognostication of pneumonia in patients with COVID-19. *Nat. Commun.* **14**, 8469 (2023).
39. Pratomo, I. P. et al. Xanthine oxidase-induced inflammatory responses in respiratory epithelial cells: a review in immunopathology of COVID-19. *Int J. Inflamm.* **2021**, 1653392 (2021).
40. Pol, K., Puhlmann, M. L. & Mars, M. Efficacy of L-arabinose in lowering glycemic and insulinemic responses: the modifying effect of starch and fat. *Foods* **11**, 157 (2022).
41. Ahmed, I., Roy, B. C., Khan, S. A., Septer, S. & Umar, S. Microbiome, metabolome and inflammatory bowel disease. *Microorganisms* **4**, 20 (2016).
42. Ursell, L. K. et al. The intestinal metabolome: an intersection between microbiota and host. *Gastroenterology* **146**, 1470–1476 (2014).
43. Teufel, R. et al. Bacterial phenylalanine and phenylacetate catabolic pathway revealed. *Proc. Natl. Acad. Sci. USA* **107**, 14390–14395 (2010).
44. Sperling, O. Human purine metabolism. in (eds De Jong, J.W.) *Myocardial Energy Metabolism,* Vol 91 (Springer, 1988).
45. Farley S. E. et al. A global lipid map reveals host dependency factors conserved across SARS-CoV-2 variants. *Nat. Commun.* **13**, 3487 (2022).
46. Van Wyngene, L., Vandewalle, J. & Libert, C. Reprogramming of basic metabolic pathways in microbial sepsis: therapeutic targets at last? *EMBO Mol. Med.* **10**, e8712 (2018).
47. Niu, Z. et al. Circulating glycerolipids, fatty liver index, and incidence of type 2 diabetes: a prospective study among Chinese. *J. Clin. Endocrinol. Metab.* **106**, 2010–2020 (2021).
48. Prentki, M. & Madiraju, S. R. Glycerolipid metabolism and signaling in health and disease. *Endocr. Rev.* **29**, 647–676 (2008).
49. Hofer, S. J. et al. Mechanisms of spermidine-induced autophagy and geroprotection. *Nat. Aging* **2**, 1112–1129 (2022).
50. Danlos et al. Metabolomic analyses of COVID-19 patients unravel stage-dependent and prognostic biomarkers. *Cell Death Dis.* **12**, 258 (2021).
51. Korbecki, J. & Bajdak-Rusinek, K. The effect of palmitic acid on inflammatory response in macrophages: an overview of molecular mechanisms. *Inflamm. Res.* **68**, 915–932 (2019).

Acknowledgements

This research was supported by EU funding within the Next Generation EU-MUR PNRR Extended Partnership initiative on Emerging Infectious Diseases (project no. PE00000007, INF-ACT) and was partially supported by an Italian Ministry-funded Project of Relevant National Interest (PRIN) focusing on the consequences of COVID-19 in the pediatric population (Project Code: E53D2300145006). V.D. received funding from the Italian Ministry of University and Research for the project CUP E53D23001520006, in the context of the Research Project of National Interest (PRIN2022); for the project CUP D93C22000890001 (ON-Foods, PE00000003) in the context of the National Recovery and Resilience Plan (NRRP); for the project PNRR-POC-2022-12376280 funded by the Italian Ministry of Health. V.D. received funding by the European Society of Pediatric Gastroenterology Hepatology, and Nutrition (ESPGHAN Research Grant 2019). V.D. received research support from the National Recovery and Resilience Plan (NRRP), Mission 4 Component 2 Investment 1.3—Call for tender No. 341 of 15 March 2022 of the Italian Ministry of University and Research, funded by the European Union—NextGenerationEU. Project code PE00000003, Concession Decree No. 1550 of 11 October 2022, adopted by the Italian Ministry of University and Research, CUP E63C22002030007, Project title "ON Foods—Research and innovation network on food and nutrition Sustainability, Safety and Security—Working ON Foods" and from the Italian Ministry of Health-Health Operational Plan Trajectory 5-Line of action "creation of an action program for the fight against malnutrition in all its forms and for the dissemination of the principles of the Mediterranean diet" (Mediterranean Diet for Human Health Lab, "MeDiHealthLab", code T5-AN-07, CUP E63C22002570006).

Author contributions

A.L.V., V.D., and L.P. performed study concept and design; A.L.V., V.D., L.P., A.Ca, M.P., and E.B. contributed to patients enrollment and provided acquisition of the data; J.T., M.L., and A.Co developed the methodology and performed the statistical analysis of the data; V.D., A.L.V., L.P., and J.T. contributed to data interpretation and writing of the paper; J.T. and A.G. provided technical and material support. All authors read and approved the final paper.

Competing interests

J.T. and M.L. are employed in a company (Theoreo Srl) or in a foundation (EIM) dealing with the development and market of diagnostic tests based on metabolomics. All other authors declare no competing interests.

Additional information

Supplementary information The online version contains Supplementary material available at https://doi.org/10.1038/s43856-026-01431-x.

Correspondence and requests for materials should be addressed to A. Lo Vecchio or A. Guarino.

Peer review information *Communications Medicine* thanks Joshua Manor and the other anonymous reviewer(s) for their contribution to the peer review of this work. A peer review file is available.